

Chapter 5

Influence of Silicon Content on the Mechanical Properties of Additively Manufactured Al-Si Alloys



Enes Sert, Philippe du Maire, Elmar Schuch, Leonhard Hitzler,
Ewald Werner, and Andreas Öchsner

Abstract One research area of additive manufacturing is material development and property optimisation, being investigated in our study through static mechanical tests. The materials tested are Al-Si alloys with 8–16 wt.% Si, without any other alloying elements. Tensile strengths achieved for the different materials are between 263 and 411 MPa. For AlSi16, the maximum tensile strength of 411 MPa was achieved at an elongation to fracture of 6.2%. Furthermore, the suitability of the individual powder batches for additive manufacturing was investigated by determining the flow function of the powder batches. Flow properties, particle size distribution and hardness were determined using additively manufactured cubes. A hardness of 149.7 HV10 was achieved for the alloy AlSi16.

Keywords Selective laser melting · Al-Si alloys · Tensile test · Flow properties · Particle size distribution

E. Sert (✉) · P. du Maire · E. Schuch · A. Öchsner
Faculty of Mechanical and Systems Engineering, Esslingen University of Applied Sciences,
73728 Esslingen, Germany
e-mail: enes.sert@hs-esslingen.de

P. du Maire
e-mail: philippe.du-maire@hs-esslingen.de

E. Schuch
e-mail: elmar.schuch@hs-esslingen.de

A. Öchsner
e-mail: andreas.oechsner@hs-esslingen.de

E. Sert · L. Hitzler · E. Werner
School of Engineering and Design, Institute of Materials Science and Mechanics of Materials,
Technical University of Munich, 85748 Garching, Germany
e-mail: hitzler@wkm.mw.tum.de

E. Werner
e-mail: werner@wkm.mw.tum.de

P. du Maire
Faculty of Aerospace Engineering, Universität der Bundeswehr München, 85748 Neubiberg,
Germany

5.1 Introduction

Additive manufacturing offers unique opportunities to produce complex components which are impossible or very difficult to realise using conventional manufacturing processes (Sert et al. 2018). The potential of additive manufacturing of aluminium alloys is already recognised in prototyping, but still holds potential in regard to the optimisation of the materials used and, above all, mass production.

AlSi10Mg represents the most frequently used alloy for selective laser melting (Drossel et al. 2018; Buchbinder et al. 2011; Buchbinder 2013) followed by AlSi12 (Siddique et al. 2015; Rashid et al. 2018). For both alloys, the mechanical properties of die-cast components are well known (Kaufman 1999). First, approaches to investigate the mechanical properties of additively manufactured Al-Si alloys under static and fatigue conditions have been carried out. AlSi10Mg and AlSi12 alloys are not optimised for additive manufacturing, as they were developed and optimised for casting (Drossel et al. 2018; Hitzler et al. 2018). The knowledge of the suitability of these alloys for additive manufacturing is therefore urgent, as in some cases significantly different properties of the material are required.

An examination of the microstructure of these alloys shows very fine-grained structures due to the high cooling rate in selective laser melting (Sert et al. 2019a, b; Olakanmi et al. 2015). In the eutectic or near-eutectic casting alloys AlSi12 and AlSi10Mg, refining alloying elements such as Na, Sr or Sb are added to achieve a fine eutectic. It is to be investigated whether these alloying elements are also necessary for additively produced Al-Si alloys or if they can be avoided. The alloys also contain other alloying elements, e.g. Fe, Mn and Cu, which are mainly added to improve process reliability during casting and may not be necessary in additive manufacturing (DIN EN 1706, 2010). An increase in the strength of additively manufactured AlSi10Mg is not achieved by precipitation hardening via post-heat treatment to the same extent as in their cast counterparts (Buchbinder et al. 2009). Solution annealing leads to coarsening of the very fine microstructure produced by additive manufacturing, especially true for the eutectically formed Si. As a result, strength decreases significantly, whilst ductility increases. Ageing at 150 °C for 10 h following additive manufacturing leads to a slightly better elongation to fracture of 6% compared to 3% in the additively manufactured state without a further loss in strength (Rowolt 2020). Furthermore, the annealing conditions strongly depend on the manufacturing parameters, e.g. the preheating temperature and the dwell time at these elevated temperatures.

Rapid cooling of melts shifts the eutectic point of Al-Si alloys to higher Si contents (Altenpohl 2005; Hanna et al. 1984). As a result, a high proportion of primary Al-Si solid solution is observed in the microstructure of additively produced AlSi12, an alloy that is eutectic at equilibrium cooling conditions (Siddique et al. 2015). The question arises at which Si content, the additively produced Al-Si alloy, shows a purely eutectic microstructure and how its proportion affects the properties of such alloys. The optimum proportions of eutectic and primary α -solid solution must be determined in order to achieve an optimum balance of strength and ductility, since

a minimum proportion of primary α -Al solid solution is required to ensure ductility. The fine-grained microstructure achieved in additive manufacturing gives hope to reach this goal.

Accordingly, from a technical point of view, a strength–ductility-optimised and wear-resistant aluminium alloy without an addition of expensive or structurally weakening alloying elements could be derived.

In this study, five different Al-Si alloys without further alloying elements are investigated. First, the quality and, thus, the applicability for additive manufacturing, specifically in laser powder bed fusion (LPBF), of the different powder batches are examined. Subsequently, hardness measurements and tensile tests are carried out. Finally, the results of these tests are compared to those of available cast aluminium alloys.

5.2 Experimental Methods

5.2.1 Sample Preparation

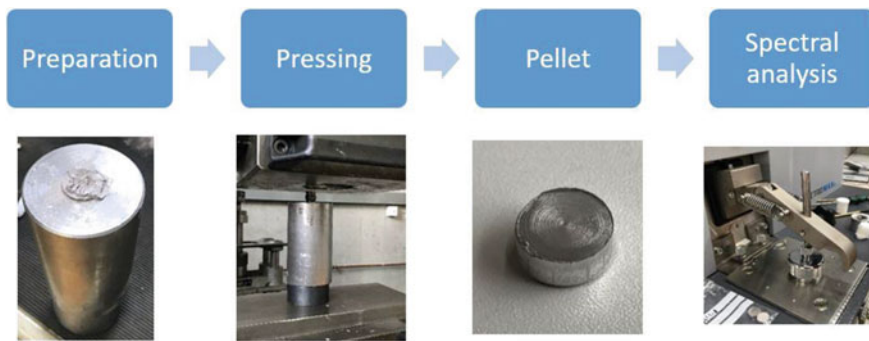
A TruPrint 3000 (TRUMPF Laser- und Systemtechnik GmbH, Ditzingen, Germany) equipped with a 500 W ytterbium fibre laser was employed for the production of the AlSi8, AlSi10, AlSi12, AlSi14 and AlSi16 samples. The laser beam diameter at the focal point was 100 μm , and the available build volume was $\text{\O} 300 \times 400 \text{ mm}^3$. An inert environment was realised with argon, with the residual oxygen content being kept below 0.1%, and the substrate plate was held at 200 °C during production. It should be mentioned that, depending on the component to be tested, the effectiveness of the heat transport via the thermal coupling of the molten bath and the sample material to the support structure varies. Given the fact that the powder bed acts like an insulation compared to solid metal due to its thermal conductivity being magnitudes lower, the thermal coupling is primarily governed by the interaction between the regulation system in the mounting plate and the component, connected via the substrate plate and the support structure. The cooling rate from layer to layer is not constant, and the effective temperature of the actively fabricated layer can deviate from the preset temperature of the installation space, becoming more pronounced with increasing height of the component. Previous experiments have shown a resulting stationary temperature of 130 °C in the powder bed, measured 10 mm above the substrate plate, at a preset temperature of 200 °C (Hitzler et al. 2017). Hence, an effective build temperature of 130 °C is assumed. For the samples (five samples per metal powder batch), five metal powder batches according to the specification of Eckart TLS GmbH with a particle size of 20–60 μm were used. The samples were produced with their longitudinal axis oriented perpendicular to the substrate plate. The process parameter set used is listed in Table 5.1. The nomenclature is in accordance with the standardisation of the samples for comprehensive experiments proposed by Buschermöhle (1995).

Table 5.1 Applied process parameters for the processing of all metal powder batches

| | Scanning speed (mm/s) | Laser power (W) | Hatch spacing (mm) | Rotation angle (°) |
|------|-----------------------|-----------------|--------------------|--------------------|
| Core | 1750 | 360 | 0.05 | 67 |

5.2.2 Chemical Analysis

The spectral analysis of the powders (SPECTROMAXx, SPECTRO Analytical Instruments GmbH) was carried out on pressed powder pellets. The pellets were produced by compressing the powder with a force of 250 kN. Three pellets were produced per batch, and three measurements were carried out on each pellet. This results in a total of nine measured values per batch, from which the averaged results were determined. Figure 5.1 shows the processing steps.

**Fig. 5.1** Process steps for the production and analysis of the pellets

5.2.3 Flowability

The analysis of the flow behaviour of the powders was carried out with a Modular Compact Rheometer (Anton Paar Germany GmbH, Ostfildern, Germany). A so-called powder cell was used. In this powder cell, the powder was fluidised by a gas volume flow, which helps to overcome gravity and interparticle forces. This is followed by the transition from static bulk material behaviour to dynamic fluid-like properties. Subsequently, the cohesive strength between powder particles was determined with the help of a two-blade stirrer. The cohesive strength is a measure of the flowability, or the internal flow resistance, of the aerated powder. During the measurement, the torque of the stirrer is recorded, and the average value of the last 20 data points is used to calculate the cohesive strength.

The flowability of a bulk material is characterised by the bulk strength σ_c as a function of the consolidation stress σ_1 and the storage time. The ratio ff_c of consolidation stress σ_1 to bulk strength σ_c is usually used as a characteristic index for flowability (Jenike 1964; Schulze 2019)

$$ff_c = \frac{\sigma_1}{\sigma_c} \quad (5.1)$$

The higher the ff_c is, i.e. the smaller the bulk strength is in relation to the consolidation stress, the better a bulk material flows. In an extension of Jenike's classification (Jenike 1964), the flow behaviour can be characterised according to Schulze as follows (Schulze 2019):

| | |
|-----------------|---------------|
| $ff_c < 1$ | not flowing |
| $1 < ff_c < 2$ | very cohesive |
| $2 < ff_c < 4$ | cohesive |
| $4 < ff_c < 10$ | easy flowing |
| $10 < ff_c$ | free flowing |

In order to classify the flowability via the flow function ff_c , it is necessary to determine the compressive strength. For this purpose, the Warren-Spring cohesion was determined using the rheometer (Ashton et al. 1965). The Warren-Spring cohesion is a measure of the flowability of compacted powders in case of cohesive powders. First, the powder is consolidated with a permeable plate, and then a stirrer with a Warren-Spring geometry is used to penetrate and shear the surface. The maximum of the shear curve represents the beginning of the flow. The resulting maximum shear stress at "failure" (i.e. where the powder starts to flow) is used to calculate the Warren-Spring cohesion. Additionally, it detects changes in formulation by first consolidating and then shearing the powder.

5.2.4 Particle Size Distribution

In order to be able to determine the particle size distribution, the image processing toolbox was used to recognise objects in images with MATLAB. The following list shows the basic steps that are carried out by the MATLAB program:

1. Reading the image into the workspace.
2. Sharpening of the image and preparation of the particle edges.
3. Converting the image into a binary form.
4. Applying a mask to split connected particles.
5. Determine the edges of the particles and draw their outlines.
6. Determine the area and perimeter of the outlined particles.
7. Calculate the maximum distance between two pixels that lie on the perimeter. This distance is the major axis of the ellipse.
8. Calculate the minor axis of the ellipse that is perpendicular to the major axis.

9. Write the values into a text file and read them into the script for statistical evaluation.

5.2.5 *Hardness*

Hardness of the built samples was determined according to the Vickers method (DIN EN ISO 6507-1) with the following settings:

- Test load: 100 N
- Dwell time: 12 s.

In order to eliminate an influence of the support structure on the test results and to ensure comparability across all materials, the surfaces of the built samples were ground in four steps (step 1: SI-C-paper, 120 grit; step 2: SI-C-paper, 320 grit; step 3: SI-C-paper, 600 grit; step 4: SI-C-paper, 1200 grit) and then polished in two steps (step 1: Sigma-paper with diamond lubricant 3 μm ; step 2: SAPHIR VIBRO with Eposil M). The hardness testing machine was manually operated, and it was ensured that the indents were located at sufficient distance from neighbouring indents. In order to be able to characterise the difference between hardness parallel and perpendicular to the layering, the hardness measurements were carried out parallel and perpendicular to the layering.

5.2.6 *Tensile Tests*

The tensile tests were carried out on a Zwick/Roell type Z100 testing machine with a load capacity of 100 kN. Before testing, the specimens were deburred with abrasive paper (Kingspor KL361JF, 320 grit, 25 mm wide) to remove possible crack initiation sites activated during mechanical loading (Sert et al. 2019b, 2020). During the tensile tests, the change in length was measured with a BTC-EXMULTI.010 multi-extensometer. In addition, Young's modulus of each specimen was determined cyclically with five measurements in the linear elastic range, for which the stress was approached to the point of the start of measurement at 10 MPa with 10 mm/min (displacement controlled) and subsequently tested at 20 MPa/s (stress controlled). The upper stress was limited to 100 MPa, and Young's modulus was evaluated between 20 and 80 MPa using the linear regression method. A full tensile test to failure was then carried out to determine the yield strength $R_{p0.2}$, the tensile strength R_m and the elongation at failure A_t according to DIN EN ISO 6892-1: 2017-02.

Table 5.2 Average chemical composition in mass percentage

| Materials | Al | STDEV | Si | STDEV | Fe | STDEV |
|-----------|--------|-------|--------|-------|-------|-------|
| AlSi8 | 91.744 | 0.201 | 7.952 | 0.219 | 0.158 | 0.007 |
| AlSi10 | 90.230 | 0.136 | 9.469 | 0.123 | 0.172 | 0.007 |
| AlSi12 | 87.994 | 0.303 | 11.774 | 0.300 | 0.153 | 0.003 |
| AlSi14 | 86.671 | 0.218 | 13.051 | 0.217 | 0.167 | 0.005 |
| AlSi16 | 84.489 | 0.388 | 15.217 | 0.385 | 0.177 | 0.003 |

STDEV is the standard deviation

5.3 Results and Discussion

5.3.1 Chemical Analysis

Through spectral analysis, the composition of the bulk material was verified (see Table 5.2). Traces (residues) of other (unwanted) elements should be avoided through the use of elemental aluminium powder. However, we found traces of Fe present in the powder batches. Unfortunately, it was not possible to procure the powder batches without Fe contamination, but since the amount of Fe was less than <0.2%, this contamination could be considered as uncritical.

5.3.2 Flowability

A rheometer with a powder cell was used to determine the cohesion strength and Warren-Spring cohesion of the individual metal powder batches. Figure 5.2 shows the cohesion strength and Fig. 5.3 the Warren-Spring cohesion.

As described in Sect. 5.2.2, the flow function ff_c is defined by the bulk strength and the consolidation stress. The bulk strength is derived from the cohesion strength. The theoretical background of this measurement is based on the Mohr–Coulomb theory on stresses in powder beds. The consolidation stress is derived from the Warren-Spring cohesion. This results in the values for the flowability listed in Table 5.3.

All powder batches are “easy flowing” according to the flow function classification and thus are suitable for additive manufacturing.

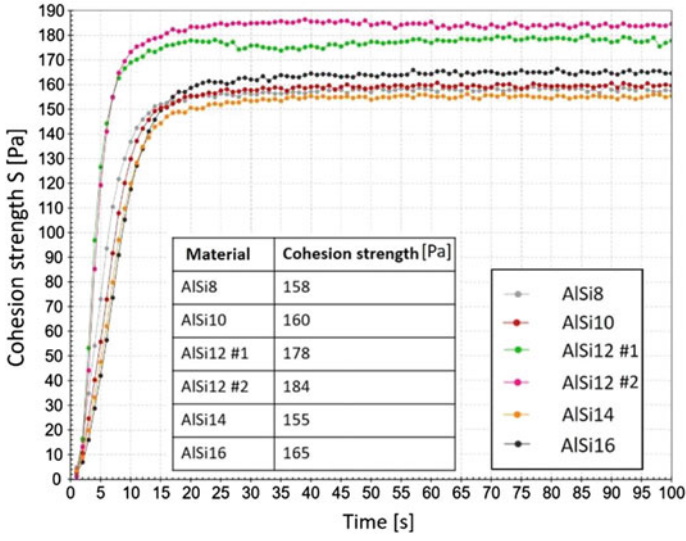


Fig. 5.2 Cohesion strength diagram for all materials

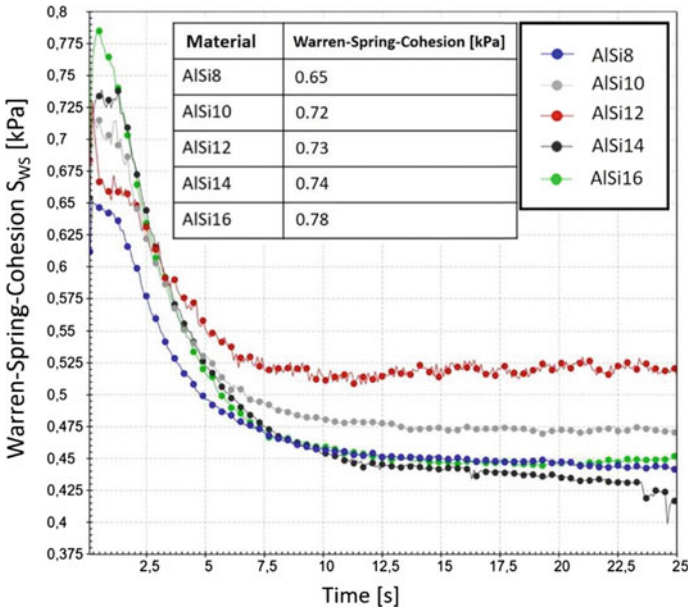


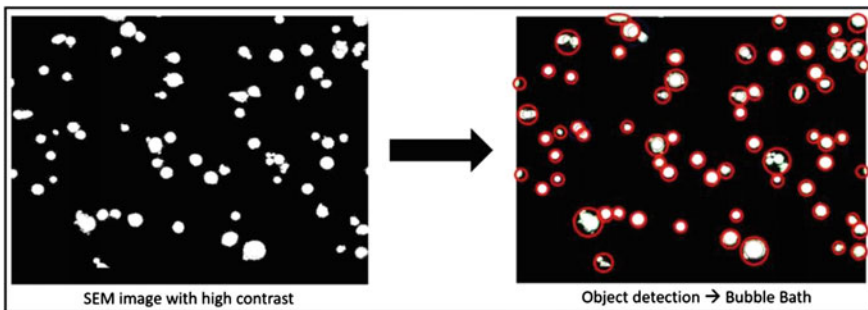
Fig. 5.3 Warren-Spring cohesion diagram for all materials

Table 5.3 Flow function ff_c determined for all five Al-Si alloys

| Alloy | ff_c |
|--------|--------|
| AlSi8 | 4.11 |
| AlSi10 | 4.50 |
| AlSi12 | 4.10 |
| AlSi14 | 4.77 |
| AlSi16 | 4.72 |

5.3.3 Particle Size Distribution

The verification of the results of the object detection algorithm is important for meaningful statistics. For this purpose, a so-called bubble bath was generated in MATLAB. The program plots white circles on a black background. It should be noted that not all circles are found on closer inspection. Circles that overlap or adhere directly to the outer edge of the image were not detected (see Fig. 5.4).

**Fig. 5.4** SEM image with high contrast and object detection “bubble bath”

The statistical evaluation of the particle size distribution is following the standard ISO 9276-1:1998. The first diagram is a histogram of the particle size. The ordinate shows the relative frequency. The length of the axes of the equivalent ellipses is plotted on the abscissa in units of μm . The second diagram is the approximated distribution of representative ellipses based on their minor axis. The ordinate shows the cumulative relative frequency and the abscissa the length of the major axes in μm . The last diagram according to ISO 9276-1:1998 is the continuous distribution density function.

The normal distribution function of the powder batch AlSi8 according to ISO 9276-1:1998 is shown schematically in Fig. 5.5. The values for all powder batches are listed in Table 5.4. Depending on the consideration of the STDEV, the particular value of the minor axis might get larger than the particular value of the major axis. Thus, the naming should be changed in such a case from minor to major axis.

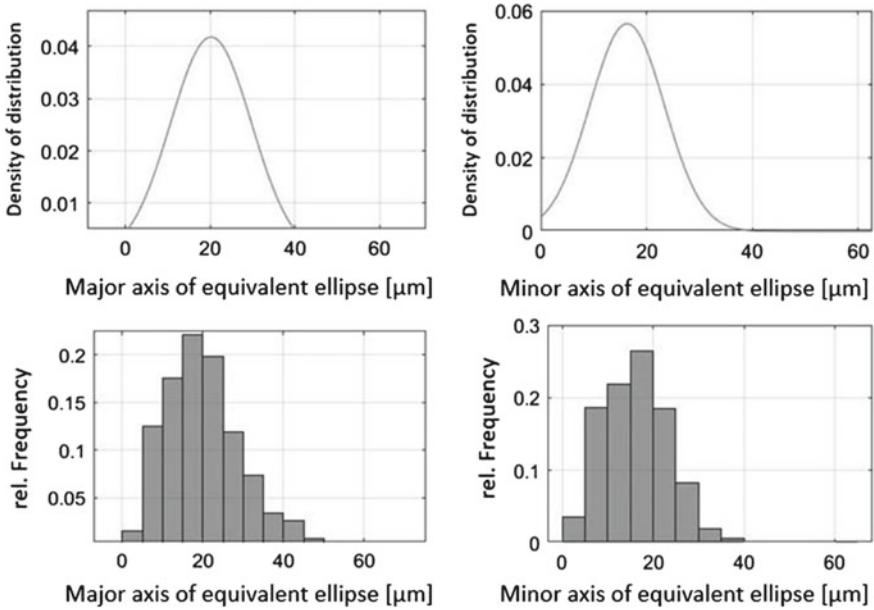


Fig. 5.5 Schematic representation of the particle size distribution of AlSi8 according to the normal distribution function

Table 5.4 Determined particle sizes of all powder batches

| Materials | Average major axis of equivalent ellipse (μm) | STDEV | Average minor axis of equivalent ellipse (μm) | STDEV |
|-----------|---|-------|---|-------|
| AlSi8 | 20.2 | 9.6 | 16.3 | 7.1 |
| AlSi10 | 18.9 | 10.8 | 15.3 | 8.7 |
| AlSi12 | 40.5 | 18.4 | 33.7 | 14.9 |
| AlSi14 | 15.3 | 10.7 | 12.4 | 8.3 |
| AlSi16 | 11.5 | 5.4 | 9.1 | 4.1 |

STDEV is the standard deviation

5.3.4 Hardness

Hardness is often employed to estimate the wear resistance of materials. The results of the hardness measurements, performed parallel and perpendicular to the layers, are shown in Fig. 5.6.

The powder batches AlSi8 and AlSi10 are hypoeutectic, whilst AlSi14 and AlSi16 are hypereutectic alloys. The powder batch AlSi12 is the near-eutectic alloy. Comparing the hardness values of the individual powder batches, it is evident that hardness increases with silicon content. The near-eutectic AlSi12 alloy has similar hardness values as the hypereutectic AlSi14 alloy. Sert et al. (2019a) investigated the

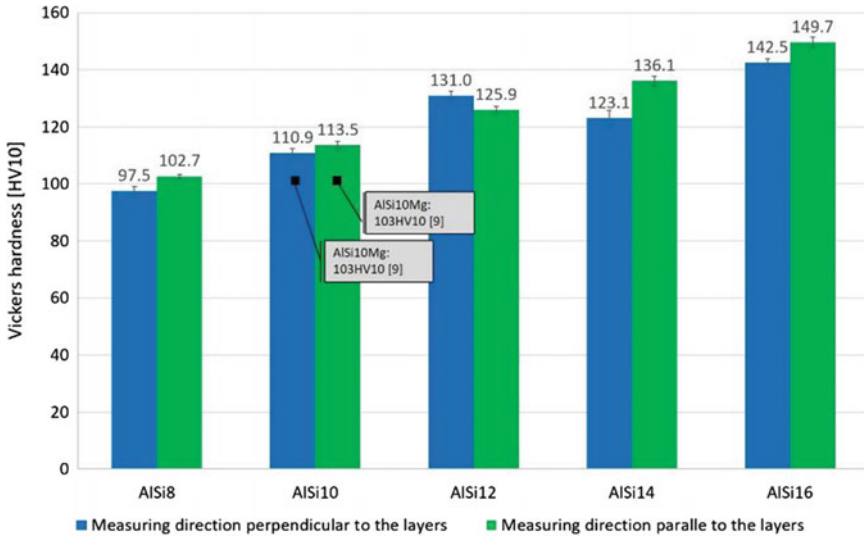


Fig. 5.6 Hardness results of the Al-Si alloys in perpendicular and parallel directions to the layers

hardness of the alloy AISi10Mg containing the common alloying elements. Hardness values of 103HV10 were determined in both perpendicular and parallel directions. Comparing the results with this current study, the hardness of the materials investigated in the study at hand is about 10% higher.

5.3.5 Tensile Properties

The results of tensile tests are given in Table 5.5. Similar to the hardness results, tensile strength increases with silicon content, whilst the elongation at failure decreases.

Table 5.5 Average results for mechanical properties; tensile tests according to DIN EN ISO 6892-1: 2017-02 measured at room temperature

| Materials | Young’s modulus E (GPa) | | Yield strength $R_{p0.2}$ (MPa) | | Ultimate tensile strength R_m (MPa) | | Elongation at failure A_t (%) | |
|-----------|---------------------------|-------|---------------------------------|-------|---------------------------------------|-------|---------------------------------|-------|
| | Average | STDEV | Average | STDEV | Average | STDEV | Average | STDEV |
| AISI8 | 68.4 | 0.3 | 200 | 0.2 | 263 | 0.5 | 10 | 1.2 |
| AISI10 | 70.2 | 0.3 | 212 | 0.7 | 307 | 0.6 | 8.5 | 0.3 |
| AISI12 | 72.3 | 0.1 | 233 | 1.7 | 341 | 0.9 | 7.5 | 1.0 |
| AISI14 | 72.6 | 0.4 | 251 | 2.1 | 376 | 4.2 | 5.1 | 1.2 |
| AISI16 | 73.9 | 0.3 | 276 | 0.9 | 411 | 0.9 | 6.2 | 0.3 |

STDEV is the standard deviation

Table 5.6 Comparison of strength values of AlSi10 determined in this study, whilst those reposted in literature for AlSi10Mg

| Study | Young's modulus E (GPa) | Yield strength $R_{p0.2}$ (MPa) | Ultimate tensile strength R_m (MPa) | Elongation at failure A_t (%) |
|-----------------------------|------------------------------|------------------------------------|---|------------------------------------|
| | Average | Average | Average | Average |
| Aboukair et al. (2016) | 77.0 | 268 | 333 | 1.4 |
| Aversa et al. (2017) | – | 246 | 362 | 4.4 |
| Buchbinder et al. (2015) | – | 150 | 250 | 4.0 |
| Hitzler et al. (2017) | 70.4 | 209 | 357 | 3.2 |
| This study | 70.2 | 212 | 307 | 8.5 |

The aim of this study is to investigate the influence of the silicon content on the mechanical properties. Furthermore, a comparison can be made between AlSi10Mg containing the common alloying elements and AlSi10 without alloying elements investigated in this study, as given in Table 5.6.

The chemical composition of the AlSi10Mg alloy influences the mechanical, physical and casting properties. The following can be reported:

- Magnesium (Mg) contributes mainly to the strength of AlSiMg alloys. The formation of precipitation phases during natural or artificial ageing significantly increases strength through the mechanism of precipitation hardening. In addition to the strength properties, hardness also increases with magnesium content. In contrast, the elongation at failure decreases with the content of Mg (Ostermann 2007; Ross and Maile 2002).
- Copper (Cu) improves the machining properties, but a too high copper content leads to a reduction in corrosion resistance and ductility (Tschirnich 2005).
- Manganese (Mn) is used to minimise mould adhesion during die casting. Furthermore, additions above 0.8% degrade mechanical properties as well as castability (Kitaoka 1995).
- Sodium (Na) and strontium (Sr) refine the residual eutectic (eutectic silicon), resulting in a fine-grained structure. The shape of Si particles changes from coarse plates to fine fibres (Closset and Gruzleski 1982).

Manganese is used to improve casting. In additive manufacturing, there is no casting mould; thus, alloying elements that reduce the adhesion of the component on the casting mould can be avoided. The addition of Cu can also be avoided in additive manufacturing, as the problem of lubrication is considered to be less important for higher Si contents. In addition, additive manufacturing is used for near-net-shape production, where machining is minimised as far as possible. Due to the high cooling rates of 10^6 – 10^8 K/s achieved in the laser powder bed fusion, LPBF materials have

extremely fine microstructures, which leads to excellent static mechanical properties in materials that are not prone to stress cracking at high cooling rates. Hence, refining elements such as Na and Sr also can be avoided.

5.4 Conclusions

The basis of this study is Al-Si alloys that exclude the common alloying elements Mg, Cu, Mn, Na and Sr. Powders from these alloys were investigated rheologically to investigate their applicability in selective laser melting. Furthermore, the influence of the silicon content on the strength properties was determined. The following conclusions can be drawn from the results:

1. The exclusion of the alloying elements Mg, Cu, Mn, Na and Sr has no negative influence on the flowability of the powder batches, and therefore, such powders are suitable for selective laser melting.
2. Hardness measurements perpendicular and parallel to the layers showed no significant differences, which seems to be a direct consequence of the homogeneous microstructure.
3. It was found that an increase in silicon content significantly affects strength properties. For example, AlSi16 has a tensile strength of 411 MPa and an elongation to failure of 6.2%.
4. The elongation to failure was also influenced by the silicon content. The elongation to failure decreased continuously from AlSi8 to AlSi14. For AlSi16, an increase in ductility could be observed. This increase will be examined in more detail in ongoing investigations.

Acknowledgements The authors thank BKL Lasertechnik GmbH for producing the samples and Anton Paar GmbH for making the rheometer tests possible and for sharing their knowledge.

This project is supported by the Federal Ministry for Economic Affairs and Climate Action (BMWK) on the basis of a decision by the German Bundestag.

References

- Aboulkhair NT, Maskery I, Tuck C et al (2016) The microstructure and mechanical properties of selectively laser melted AlSi10Mg: the effect of a conventional T6-like heat treatment. *Mater Sci Eng* 667:139–146
- Altenpohl DG (2005) Aluminium von innen: das Profil eines modernen Metalles, 5. Neubearbeitete und erweiterte Auflage. Aluminium-Verlag, Düsseldorf
- Ashton MD, Cheng DCH, Farley R et al (1965) Some investigations into the strength and flow properties of powder. *Rheol Acta* 4:206–218
- Aversa A, Lorusso M, Trevisan F et al (2017) Effect of process and post-process conditions on the mechanical properties of an A357 alloy produced via laser powder bed fusion. *Metals* 7(2):68

- Buchbinder D (2013) Selective Laser Melting von Aluminiumgusslegierungen. Dissertation, RWTH Aachen
- Buchbinder D, Meiners W, Wissenbach K et al (2009) Rapid manufacturing of aluminium parts for serial production via selective laser melting (SLM). In: 4th international conference on rapid manufacturing, Loughborough
- Buchbinder D, Meiners W, Brandl E et al (2011) Abschlussbericht—Generative Fertigung von Aluminiumbauteilen für die Serienproduktion. Fraunhofer ILT
- Buchbinder D, Meiners W, Wissenbach K et al (2015) Selective laser melting of aluminum die-cast alloy—correlations between process parameters, solidification conditions, and resulting mechanical properties. *J Laser Appl* 27(S2):S29205
- Buschermöhle H (1995) Vereinheitlichung von Proben für Schwingversuche: Abschlussbericht. FKM-Verlag, Frankfurt a.M.
- Closset B, Gruzleski JE (1982) Structure and properties of hypoeutectic Al-Si-Mg alloys modified with pure strontium. *Metall Mater Trans A* 13(6):945–951
- (DIN) Deutsches Institut für Normung e.V., DIN EN 1706 (2010) Aluminium und Aluminiumlegierungen—Gussstücke—Chemische Zusammensetzung und mechanische Eigenschaften. Beuth, Berlin
- Drossel G, Friedrich S, Kammer C et al (2018) Das Aluminium Taschenbuch 2: Umformen, Gießen, Oberflächenbehandlung, Recycling, 17. Auflage. Beuth, Berlin
- Hanna MD, Lu S-Z, Hellawell A (1984) Modification in the aluminum silicon system. *Metall Trans A* 15(3):459–469
- Hitzler L, Janousch C, Schanz J et al (2017) Direction and location dependency of selective laser melted AlSi10Mg specimens. *J Mater Process Technol* 243:48–61
- Hitzler L, Merkel M, Hall W et al (2018) A review of metal fabricated with laser- and powder-based additive manufacturing techniques: process, nomenclature, materials, achievable properties, and its utilization in the medical sector. *Adv Eng Mater* 20(5):1700658
- Jenike AW (1964) Storage and flow of solids, Bull. No. 123. Engineering Experiment Station, University of Utah, Salt Lake City
- Kaufman JG (1999) Properties of aluminum alloys tensile creep and fatigue data at high and low temperatures. ASM International Materials Park, Ohio
- Kitaoka S (1995) Wear resistant cast aluminium alloy and process of producing same. Patentschrift EP 0 672 760 A1
- Olakanmi EO, Cochrane RF, Dalgarno KW (2015) A review on selective laser sintering/melting (SLS/SLM) of aluminium alloy powders: processing, microstructure, and properties. *Prog Mater Sci* 74:401–477
- Ostermann F (2007) Anwendungstechnologie Aluminium. Springer Verlag
- Rashid R, Masood S, Ruan D et al (2018) Effect of energy per layer on the anisotropy of selective laser melted AlSi12 aluminium alloy. *Addit Manuf* 22:426–439
- Ross E, Maile K (2002) Werkstoffe für Ingenieure—Grundlagen, Anwendungen, Prüfungen. Springer Verlag
- Rowolt C (2020) Untersuchungen zur Wärmebehandlung additiv gefertigter, metallischer Bauteile auf Basis von in-situ Analysen der Phasenumwandlungen. Dissertation, University of Rostock
- Schulze D (2019) Fließigenschaften von Schüttgütern. In: Pulver und Schüttgüter: Fließigenschaften und Handhabung. Springer Berlin Heidelberg, pp 53–98
- Sert E, Hitzler L, Merkel M et al (2018) Entwicklung von topologieoptimierten Adapterelementen für die Fertigung mittels additiver Verfahren: Vereinigung von reinelektrischem Antriebsstrang mit konventionellem Chassis. *Mater Sci Technol* 49(5):674–682
- Sert E, Hitzler L, Heine B et al (2019a) Influence of the heat treatment on the microstructure and hardness of additively manufactured AlSi10Mg samples. *Pract Metallogr* 56(2):91–105
- Sert E, Schuch E, Öchsner A et al (2019b) Tensile strength performance with determination of the Poisson's ratio of additively manufactured AlSi10Mg samples. *Mater Sci Technol* 50(5):539–545
- Sert E, Hitzler L, Hafenstein S et al (2020) Tensile and compressive behaviour of additively manufactured AlSi10Mg samples. *Prog Addit Manuf* 5(3):305–313

- Siddique S, Imran M, Walther F (2015) Influence of process-induced microstructure and imperfections on mechanical properties of AlSi12 processed by selective laser melting. *J Mater Process Technol* 221:205–213
- Tschirnich M (2005) Einsatz neuer Strategien bei der Werkstoffmodellierung von Aluminiumlegierungen in der Warmumformung. Dissertation, RWTH Aachen